3D SEISMOGRAMS IN 2.5D HETEROGENEOUS STRUCTURES

T. Feskova, J. Miksat, T. M. Müller and F. Wenzel

email: *Tatiana.Feskova@stud.uni-karlsruhe.de, Joachim.Miksat@gpi.uni-karlsruhe.de, Tobias.Mueller@gpi.uni-karlsruhe.de, Friedemann.Wenzel@gpi.uni-karlsruhe.de*

keywords: *finite differences – ray tracing – 2.5D heterogeneous media – 2D to 3D conversion*

ABSTRACT

Finite-Difference (FD) simulations of elastic wave propagation is an important tool in geophysical research. As large-scale 3D simulations are only feasible on supercomputers or clusters and even then the simulations are limited to long periods compared to the model size, 2D FD simulations are widely-spread. Whereas in generally 3D heterogeneous structures it is not possible to infer the correct amplitude and waveform from 2D simulations, in 2.5D heterogeneous structures some inferences are possible. In particular, Vidale and Helmberger (1987) developed an approach that simulates 3D waveforms using 2D FD experiments only. However, their method requires a special FD source implementation technique which is not any longer used in nowadays FD codes. In this paper we derive a 2D to 3D mapping that can be applied on the computed waveforms from 2D experiments independent on the particular source implementation technique. The approach assumes that the travel path can be determined in the geometrical optic limit. Therefore, we present a hybrid modeling procedure involving 2D FD and ray tracing techniques. The applicability is demonstrated by numerical experiments of elastic wave propagation for models of different complexity.

INTRODUCTION

Finite-Difference (FD) simulations of wave propagation is a common tool in geophysical research. In seismology, wave propagation for earthquakes is simulated in order to understand the ground motion of past earthquakes and to estimate the threat of future earthquakes (e.g. Furumura and Kennett, 2005; Miksat et al., 2005; Graves and Wald, 1998; Olsen, 2000). In exploration seismology the FD method is used for reservoir modeling, survey planning (e.g.Lecomte et al. (2004)). Despite the growing computer capacities during the last decade 2D FD simulations are widely used, as 3D simulations are limited to long wavelength compared to the model size. For example, large scale simulations of earthquake wave propagation calculated on the world's largest computers are limited to frequencies below 1 Hz (Furumura and Kennett, 2005), which is far below the range of engineering interest (f$<$ 15 Hz). Hence, 2D FD simulations are routinely applied to explore a larger frequency range or large scale models (e.g., Furumura and Kennett, 2005; Benites and Olsen, 2005; Kebeasy and Husebye, 2003). However, most of these studies focus on the simulated travel times and relative amplitudes whereas the calculation of absolute amplitudes is neglected. This is rooted in the fact that the amplitudes for whole space (3D) wave propagation cannot be directly simulated with a 2D FD method, because the 3D solution of the equation of motion differs in phase and geometrical spreading from the 2D solution. However, the calculation of absolute amplitudes is, especially in seismology, a crucial parameter as the absolute value of ground shaking is related to the resulting damage.

In many instances, the spatial distribution of elastic properties in earth models can be approximated by a 2.5D heterogeneous structure. This fact prompted the idea that 3D seismograms in 2.5D heterogeneous structures could be obtained from 2D simulations only provided that the difference in the geometrical spreading is properly accounted for. Using the correspondence between a 2D line source and a 3D point

source in homogeneous media Vidale and Helmberger (1987) developed a correction procedure which translates 2D FD seismograms into 3D seismograms. In particular, They derived the following formula to simulate a displacement seismogram resulting from a point source in 3D, u_i^{3D}, using the 2D FD displacement seismogram, u_i^{2D}:

$$u_i^{3D} = \frac{1}{\sqrt{r}} \frac{d}{dt} \left(\frac{1}{\sqrt{t}} * u_i^{2D} \right), \tag{1}$$

where r is the travel path of the wave. However, it is important to note that the method of Vidale and Helmberger (1987) is dependent on the source implementation technique, which was invented by Alterman and Karal (1968) and which was widely used in the first FD codes. This means that eq. (1) is only valid for the particular source implementation technique used by Vidale et al. (1985) and Vidale and Helmberger (1987), which imposes the whole space, line source, first term asymptotic GRT (generalized ray theory) solution on the source grid points. Today, most FD codes do not use this technique. Instead, sources are implemented by adding displacement or stress tensor components to the corresponding grid nodes (Graves, 1996; Coutant et al., 1995; Karrenbach, 1995; Bohlen, 2002). Consequently, the procedure ofVidale and Helmberger (1987) cannot be applied without further modification to simulate 3D seismograms. Nevertheless, equation (1) is used from time to time to transform 2D into 3D seismograms Igel et al. (2002); Olsen et al. (1996).

In this paper, we develop a procedure that allows to compute accurate 3D seismograms in 2.5D heterogeneous structures from 2D FD calculations with any source implementation technique. Starting from the equivalence between a point source in 2D space and a line source in 3D space, we derive a time-domain conversion operator that achieves the desired 2D to 3D conversion. This operator involves the exact travel path of the wave which can be determined in the geometrical optic approximation. Therefore, we suggest a hybrid method that combines 2D FD and ray tracing. The latter allows the calculation of the exact travel path for different phases in the geometrical optic limit. We demonstrate the capability of the method by various numerical examples. In each example elastic wave propagation is modeled using a point source in 3D (the 'true' reference experiment) and a point source in 2D (simulated by a line source in 3D). Simulated point source seismograms in 3D are then obtained by convolving the time-domain conversion operator with the line source seismograms. The simulated 3D seismograms are compared with the corresponding 3D reference experiments. We give error estimates and discuss the limitations of the method.

THEORY

Seismograms of the displacement or particle velocity due to line sources in 3D space have an infinitely long tail and the far-field geometrical spreading is proportional to $1/\sqrt{R}$ as compared to $1/R$ for seismograms due to point sources in 3D space. It is well-known that in homogeneous elastic media wave propagation initiated by a point source in 2D corresponds to wave propagation for an line source in 3D. This equivalence can be exploited in order to derive a mapping between line source and point source seismograms. In order to do so, we start out with the far field Green's tensor G_{ij} in the frequency domain for an elastic, isotropic medium is given by (Hudson, 1980, p. 137):

$$\begin{aligned} G_{il}(\omega) &= \frac{1}{4\pi\rho} \left[\frac{\hat{x}_l \hat{x}_i}{\alpha^2 R} e^{i\omega R/\alpha} + \frac{(\delta_{il} - \hat{x}_i \hat{x}_i)}{\beta^2 R} e^{i\omega R/\beta} \right] \\ &= \frac{1}{4\pi\rho} \left[\frac{\hat{x}_l \hat{x}_i}{\alpha^2 R} e^{ik_\alpha R} + \frac{(\delta_{il} - \hat{x}_i \hat{x}_i)}{\beta^2 R} e^{ik_\beta R} \right], \end{aligned} \tag{2}$$

with the unit vectors $\hat{x}_l$ and $\hat{x}_i$ in l and i-direction, P-wave speed α, S-wave speed β, travel distance R and the Kronecker delta notation δ_{il}.

For simplicity the 2D to 3D conversion operator is derived for an acoustic medium. However, it is important to note that the result is also valid for the elastic case because the Green's functions for both cases involve the same wave function $\frac{e^{ikR}}{R}$ with wavenumber $k = \omega/c$ (where c is either α or β).

The Green's function for the velocity potential Ψ in the Helmholtz equation is given by:

$$G^{\text{point\_3D}}(\omega) = \frac{e^{ikR}}{4\pi R}, \tag{3}$$

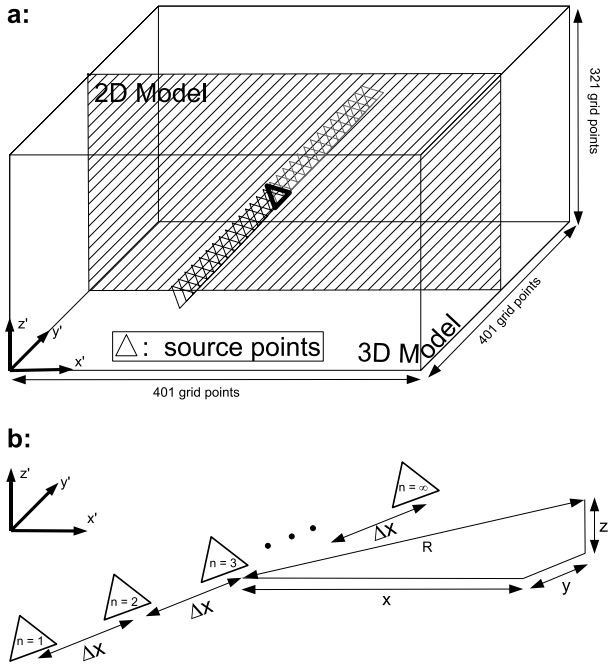

Figure 1: a: Source location within the applied 3D model. The 3D model is unaltered in y direction. Wave propagation is simulated for a line source (triangles) with 3D FD in order to get the equivalence to a 2D simulation for the marked 2D model. Further, 3D FD simulation is performed for a point source (bold triangle). b: Infinite line source in y direction with grid spacing Δx between the source nodes.

with distance R between source and receiver in cartesian coordinates:

$$R = \sqrt{x^2 + y^2 + z^2}. \tag{4}$$

The Green's function of a line source can be constructed by adding the contributions of an infinite number of aligned point sources. This is illustrated in In Fig. 1 where a large number of point sources aligned in y-direction of the computational gird with grid spacing Δx simulates a line source in y-direction. Therefore, the discrete Green's function $G^{\text{line\_3D}}$ representing the line source in Fig. 1 is given by:

$$G^{\text{line\_3D}}(\omega) = \frac{1}{4\pi} \sum_{n=1}^{\infty} \frac{e^{ik\sqrt{r^2+y^2}}}{\sqrt{r^2+y^2}}, \tag{5}$$

where $y = n\Delta x$ and $r^2 = x^2 + z^2$, which is the square of the distance in the xz-plane between source and receiver. Applying the Fresnel approximation and writing the sum as an integral, eq. (5) transforms into:

$$G^{\text{line\_3D}}(\omega) = \frac{e^{ikr}}{4\pi r} \frac{1}{\Delta x} \int_{-\infty}^{+\infty} e^{\frac{ikx^2}{2r}} dx. \tag{6}$$

The integral on the right hand side is given by:

$$\int_{-\infty}^{+\infty} e^{\frac{i\omega x^2}{2cr}} dx = \frac{e^{\frac{i\pi \text{sgn}(\omega)}{4}}}{\sqrt{|\omega|}} \sqrt{2\pi cr}, \tag{7}$$

where sgn denotes the signum function. Using eq. (7) the Green's function for a line source can be represented as:

$$G^{\text{line\_3D}}(\omega) = G^{\text{point\_3D}}(\omega) \quad C^{-1}(\omega)\,, \tag{8}$$

where

$$C^{-1}(\omega) = \frac{1}{\Delta x}\sqrt{\frac{2\pi c r}{|\omega|}} e^{\frac{i\pi \mathrm{sgn}(\omega)}{4}} \tag{9}$$

This means that the 3D line source Green's function (8) is composed out of the 3D point source Green's function (3) multiplied by the function (9). Conversely, multiplying equation (8) by the inverse of $C^{-1}(\omega)$, i.e, $C(\omega)$ yields the 3D point source Green's function expressed in terms of the 3D line source Green's function (or, equivalently, in terms of the 2D point source Green's function). Applying the inverse Fourier transform to the function $C(\omega)$ yields the time domain conversion operator

$$\tilde{C}(t) \quad = \quad \frac{\Delta x}{\pi r\sqrt{2/t}} \frac{d}{dt} \frac{H(t)}{\sqrt{t}} \,, \tag{10}$$

where H denotes the Heaviside step function. Thus, the 2D FD line source seismogram $\Psi^{\mathrm{line_2}D}(t)$ can be translated into a 3D point source seismogram $\Psi^{\mathrm{point\_3D}}$ by applying operator (10) to $\Psi^{\mathrm{line\_2D}}(t)$:

$$\Psi^{\mathrm{point\_3D}} \quad = \quad \tilde{C}(t) * \Psi^{\mathrm{line\_2D}}(t) \tag{11}$$

$$= \quad \frac{\Delta x}{\pi r\sqrt{2/t}} \left\{ \frac{d}{dt} \frac{H(t)}{\sqrt{t}} * \Psi^{\mathrm{line\_2D}}(t) \right\} \,, \tag{12}$$

where the asterisk denotes time domain convolution. Equation (12) is exact for a homogeneous acoustic medium. Equation (12) is also applicable in for the elastodynamic far field if the velocity potential is replaced by the displacment vector components.
In order to apply (12) to elastic, 2.5D heterogeneous media it requires the knowledge of the exact travel path the wave takes ($\bar{r}$). We assume that $\bar{r}$ can be approximated by the corresponding high-frequency response, that is, in the geometrical optic limit. Thus, in order to simulate 3D point source seismograms from 2D finite difference experiments we propose the following formula for the displacement components

$$u_i^{\mathrm{point\_3D}} \approx \frac{\Delta x\sqrt{t}}{\sqrt{2}\pi\bar{r}} \left\{ \frac{d}{dt} \frac{H(t)}{\sqrt{t}} * u_i^{\mathrm{line\_2D}}(t) \right\}, \tag{13}$$

where exact travel path is determined in the geometrical optic limit. This means that in addition to a 2D finite difference solver of the elastodynamic wave equation, a finite difference solver of the eikonal equation or a ray tracing algorithm is required. We expect that formula (13) remains valid as long as $\bar{r}$ can be accurately evaluated in the geometrical optic limit. For an extensive review of the applicability of the geometrical optic approximation we refer to Kravtsov and Orlov (1990). The applicability of equation (13) in 2.5D heterogeneous media is demonstrated with help of several examples.

MODELLING TECHNIQUES

The simulations are carried out by applying the 3D FD code of Olsen (1994) which is frequently used for earthquake wave propagation simulations (e.g., Olsen, 2000; Gottschämmer et al., 2002; Miksat et al., 2005; Oth et al., 2007). The code is of 4th order in space and 2nd order in time. To validate our proposed correction method, we apply 3D simulations with line sources in order to generate the equivalent to a 2D simulation. The results are corrected according to eq. (12) and compared with a 3D FD simulation for a point source. The 3D models are 2.5D models, as they are not altered in y direction. The line sources are parallel to the y-axis of the model (see Fig. 1). The considered 2D slice corresponds to the xz plane at grid node number 201 in y direction. The modeling parameters are given in Table 1. To minimize numerical dispersion errors, at least 11 points per minimum wavelength are used for the modeling. Consequently, all seismograms are filtered with a four pole Butterworth lowpass filter with cutoff frequency of 0.5 Hz. A double couple stress source with a Ricker wavelet is added to the corresponding source grid points.
In order to get the length of the travel path needed in order to apply (12) we use a two-point ray tracing algorithm.

Table 1: Modeling parameters

Spatial discretization dx (km)	0.50
Number of grid points (x-direction)	401
Number of grid points (y-direction)	401
Number of grid points (z-direction)	321
Horizontal extension in x-direction (km)	200
Horizontal extension in y-direction (km)	200
Vertical extension in z-direction (km)	159
Temporal discretization dt (ms)	17
Number of time steps	7000
Simulation time (s)	119

EXAMPLES

In this section the derived method is applied to the modeling of wave propagation within four different structural models. We compare simulated 3D waveforms obtained with the hybrid approach to the results obtained from 3D FD point source simulations. The 2D to 3D conversion are performed for straight lined (source-receiver) travel paths and actual paths calculated by the ray tracer. The relative error is calculated by comparing the maximum phase amplitudes of the 3D FD point source (A^{3D}_{max}) and the converted seismograms (A^{conv}_{max}):

$$\text{relative error} = \frac{\left|A^{conv}_{max} - A^{3D}_{max}\right|}{|A^{3D}_{max}|}. \tag{14}$$

Homogeneous medium

First, we test the correction procedure for the simplest case: a homogeneous structure where all trave paths are straight lines. The source is located in a depth of 70 km and the seismograms are compared at a surface point with an offset of 30 km. Consequently, the straight line travel path length is 72.5 km. The comparison shows an excellent fit (Fig. 2). The small deviations are most probably produced by the discrete nature of a line source in FD simulations compared to real continuous line sources. By comparing the maximum amplitudes of the point source and corrected line source, we find deviations of 2%, 1.2% and 5.3 % for the x-,y- and z-component, respectively. This should be regarded as the intrinsic error of FD algorithm probably related to numerical dispersion.

Layered structure – internal multiple

Fig. 3 displays the 2D slice of the layered model. The source is located in a depth of 70 km at x = 0 km. First the direct S-phase at station A is examined. Fig. 3 shows the corresponding ray path calculated with the ray tracer. The length of the straight line travel path is 139 km and144 km for the real ray path. The resulting seismograms for station A are shown in Fig. 4. In our example, the S wave shows only on the y-component a clearly visible onset with an amplitude about ten times larger than of the x- and z-components. For the y-component, the relative error (see 14) is 2.2% for the straight line approximation and 1.7 % for thhybrid method. There is almost no difference between the correction applied with the straight line approximation and the real travel path length. Therefore, the straight line approximation is a valid assumption for small deviations of the travel path from a straight line. Next, we look at a phase which is trapped in the low velocity channel and is recorded at station B (Fig. 5). In this case the computed length of the ray path is 136 km and 81 km for a straight line between source and station B. Here, the information from the ray tracer is crucial in order to perform the correction. For the x- and y-component, which shows the largest amplitudes for the trapped phase arrival, the correction fits to the 3D results (relative errors of 3.4% and 11 %, respectively). These errors are larger than the intrinsic errors found for the homogeneous model. This may be explained by the fact that due to the complex underground structure the considered

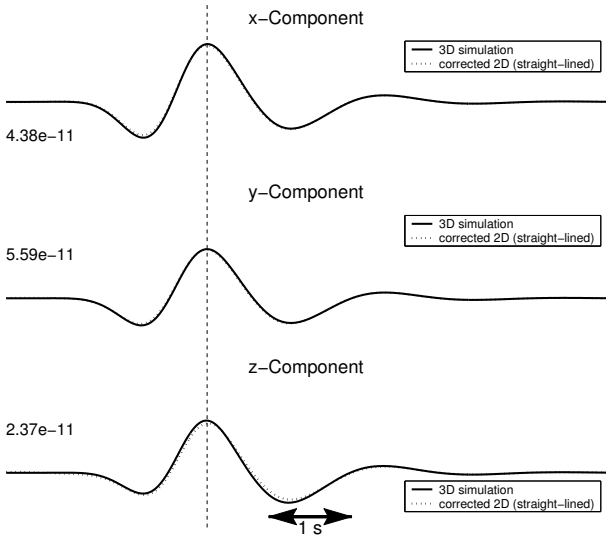

Figure 2: Comparison of a simulation of a point source (solid) with the corrected simulation of a line source (dashed) for a homogeneous model. The relative errors of the maximum amplitudes are 2%, 1.2% and 5.3 % for the x-,y- and z-component, respectively.

S-phase contains also small P- or S-phases, which traveled different paths but arrive at the same time. In this case, the assumption made for the conversion is not completely valid.

Lense structure – wavefield focusing

A buried lense structure causes strong deviations from straight line ray paths and such structures are able to focus rays from different directions. Such an extreme case is examined in this section. Fig. 6 shows the velocity structure of the model. The source is located in a depth of 130 km and the buried structure are almost symmetric to the x = 0 km. We test the procedure for a station at x = 0 km, where the marked ray paths in Fig. 6 coincide. The 3D point source simulation and the corrected 3D line source simulation is compared in Fig. 7. Here, we compare the direct P-wave arrivals, rather than the S-phases. In Fig. 7 only the x- and z-components are shown, as there is no P-wave on the y-component for 2D modeling and for 3D modeling with line sources. The relative errors of the maximum amplitudes of the x-component are 13 % for the straight line and 2 % for the hybrid approach. For the z-component the relative error are 7.8 % (straight line approximation) and 3 % (hybrid method). This example emphasizes the need for the hybrid method for complex underground structures that strongly deflect the direct ray path.

Real subsurface structure

Here, the correction procedure is tested for a earthquake modeling application. Fig. 8 shows a slice through the 3D underground structure of Romania based on (Martin et al., 2005). A linear trend is over-imposed on the known subsurface structures in order to enhance the complexity of the model. An extended study of 2D FD wave propagation modeling of the strong Vrancea earthquakes in Romania was performed by (Miksat, 2006). The correction is shown for a station at x = 83 km, the ray path is altered by the strong curvature of the basin structure and for a station at x=83 km. The straight line and real travel paths lengths are 114 km and 109 km, respectively. We compare our conversion (12) with conversion (1) given by Vidale and Helmberger (1987), which was used by Igel et al. (2002); Olsen et al. (1996). The relative error is 3.8 %, 5.7 % and 6.0 % (x-, y- and z-component) for our hybrid approach and 46 %, 47 % and 47 % (x-, y- and z-component) for the conversion given by Vidale and Helmberger (1987).

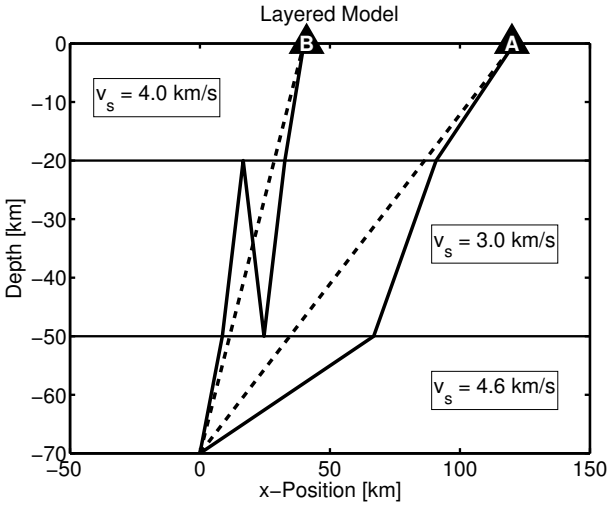

Figure 3: Model with three horizontal layers. The S-wave velocity of the middle layer is the lower than for the top and bottom layers. First the correction is examined for the direct S-wave at station A. The second case evaluates the correction for the S wave which was trapped in the low velocity channel and finally observed at station B. The solid lines depict the travel paths and the dashed lines their straight line approximations.

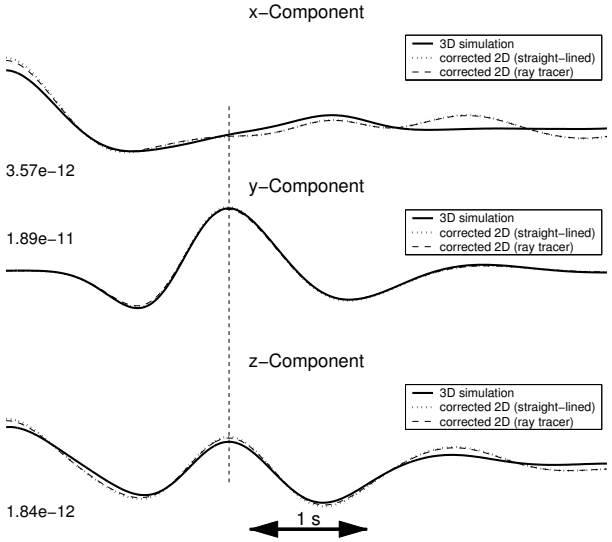

Figure 4: Comparison of the point source and corrected line source simulations for the direct S-wave at station A (see Fig. 3). The straight line and real travel path lengths are 139 km and 144 km, respectively. For such small differences compared to the total travel path length, a straight line travel paths can be adopted for the correction.

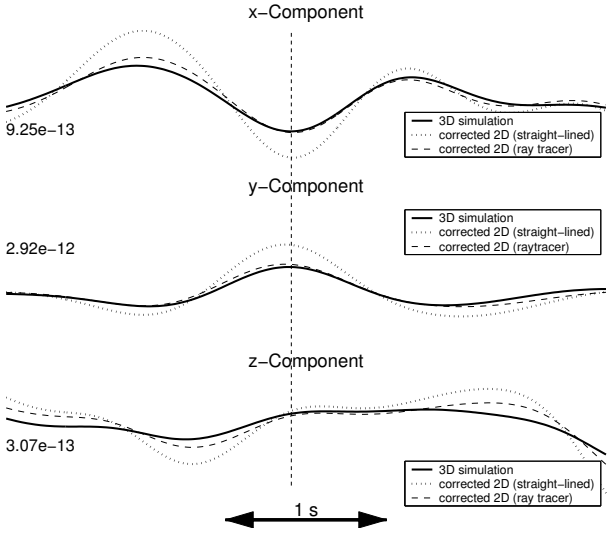

Figure 5: Comparison for the S-wave that was trapped for one cycle in the velocity channel (see Fig. 3). The seismograms are evaluated at station B about. The assumption of a straight line path (dotted) fails here. The correction with the travel path calculated by ray tracing gives a good fit between point (solid) and corrected line (dashed) source simulations.

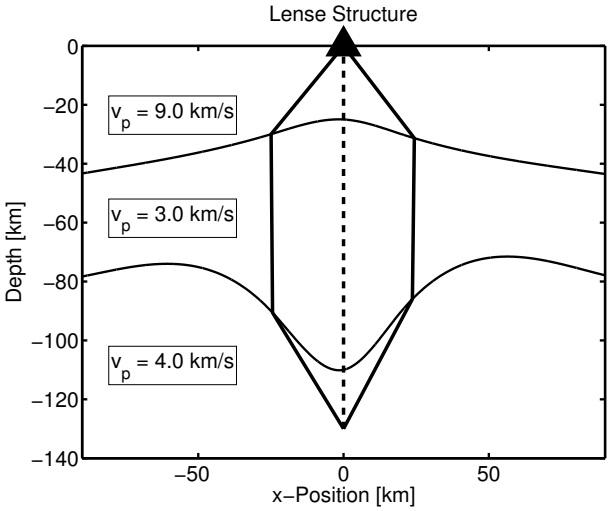

Figure 6: Model with a buried lense like structure. This structure produced large deviations from straight line ray paths.

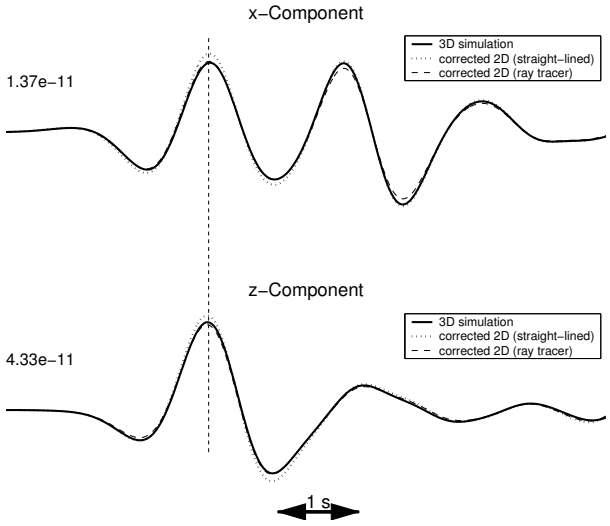

Figure 7: Modeled point source (solid) and corrected line source (dashed and dotted) simulation at 0 km (see Fig. 6) for the lense like structure. At 0 km, the rays arrive from different directions and coincide. Even though the fit is good for both cases, straight line (dotted) and real (dashed) travel path, the information from the ray tracer is crucial in order to obtain an excellent fit.

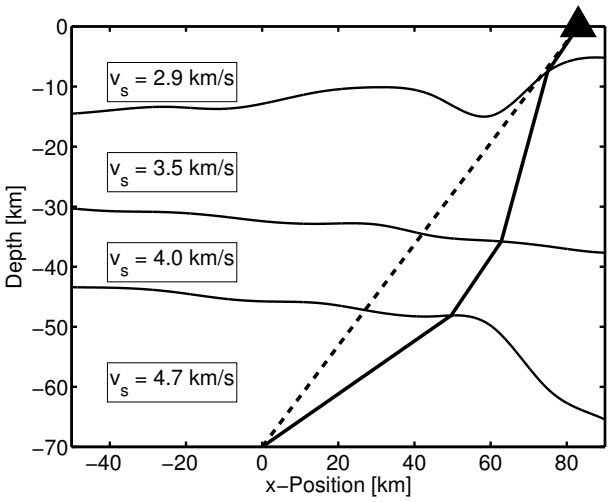

Figure 8: The correction procedure is tested for a realistic subsurface structure. This structure is based on Martin et al. (2006). To enhance the complexity of the model, a linear trend is over-imposed on the known subsurface structures. The seismograms are evaluated at x = 83 km (Fig. 9).

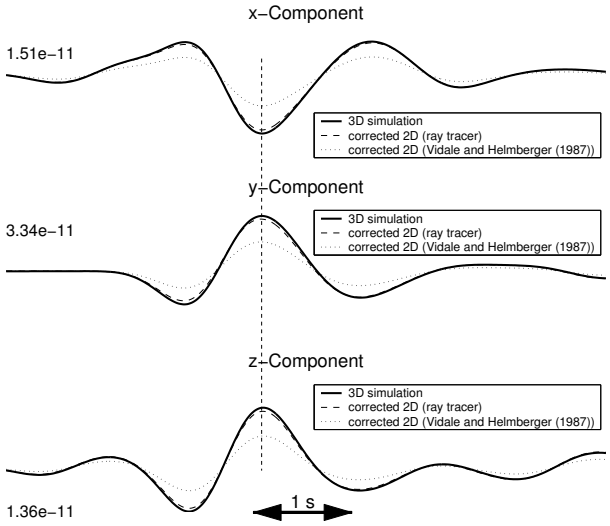

Figure 9: Comparison of the point source and corrected line source seismogram after our hybrid approach and the conversion given by Vidale and Helmberger (1987) at x = 83 km (see Fig. 8) for a realistic subsurface structure.

DISCUSSION

The examples show that the proposed method can be applied in a range of scenarios. A general limitation is the restriction to 2.5D heterogeneous models. Wave propagation within complicated 3D models and the corresponding 3D effects cannot be modeled with a 2D approach. However, in many cases the real underground structure can be approximated by a 2.5D structure and in these cases, the correction method allows a fast calculation of waveforms and absolute amplitudes without time and memory intensive 3D simulations. For very complicated ray paths, such as trapped or strongly deflected rays, the hybrid approach of FD and ray tracing allows a reliable calculation of the 3D seismograms. By calculating many different rays (reflections and refractions) for one location and the corresponding arrival times a 2D FD seismogram as a whole can be properly corrected. A further limitation is observed for the layered structure. If the considered phase is contaminated with other phases, the conversion cannot be applied correctly because the travel paths of these phases differ. In these cases the quality of the conversion procedure depends on the relative amplitude of the considered phase to the contaminating phases.

CONCLUSIONS

We propose a hybrid modeling method to simulate 3D waveforms and amplitudes based on seismograms calculated with 2D FD and on the actual ray paths determined by ray tracing. The approach is based on the equivalence of point sources in 2D FD modeling and line source in 3D modeling. Compared to formerly published correction procedures there is no limitation on the particular FD code. We showed by comparison of 3D and corrected 2D seismograms for models of various complexities the applicability of the correction method to underground structures of realistic velocity contrasts and complexity. As 2D FD full waveform calculations are less time and computer memory intensive compared to 3D simulations, this method allows a quick calculation of accurate waveforms and amplitudes for 2.5D heterogeneous structures.

ACKNOWLEDGMENTS

This research was funded by the Deutsche Forschungsgemeinschaft (DFG) through the Collaborative Research Centre 461 ‘Strong Earthquakes: A Challenge for Geosciences and Civil Engineering’ (CRC 461) and contract MU1725/1-3. We thank J. Mann for providing the 2-point ray tracer and Tatiana Feskova for doing the ray tracing and displaying the results. We also thank K. B. Olsen for providing the 3D FD code.

REFERENCES

Benites, R. and Olsen, K. B. (2005). Modeling strong ground motion in the Wellington metropolitan area, New Zealand. *Bull. Seism. Soc. Am.*, 95(6):2180–2196.

Bohlen, T. (2002). Parallel 3-d viscoelastic finite-difference seismic modelling. *Computers @ Geopsciences*, 28(8):887–899.

Coutant, O., Virieux, J., and Zollo, A. (1995). Numerical source implementation in a 2D finite difference scheme for wave propagation. *Bull. Seism. Soc. Am.*, 85(5):1507–1512.

Furumura, T. and Kennett, K. (2005). Subduction zone guided waves and the heterogeneity structure of the subducted plate: Intensity anomalies in northern Japan. *J. Geophys. Res.*, 110:B10302.

Gottschämmer, E., Wenzel, F., Wust-Bloch, H., and Ben-Avraham, Z. (2002). Earthquake modeling in the dead sea basin. *Geophys. Res. Lett.*, 29(12):1567, doi:10.1029/2001GL013800.

Graves, R. W. (1996). Simulating seismic wave propagation in 3D elastic media using staggered-grid finite differences. *Bull. Seism. Soc. Am.*, 86(4):1091–1106.

Graves, R. W. and Wald, D. J. (1998). Observed and simulated ground motions in the San Bernardino basin region for the Hector Mine, California, earthquake. *Bull. Seism. Soc. Am.*, 94(1):131–146.

Hudson, J. A. (1980). *The excitation and propagation of elastic waves*. Cambridge University Press.

Igel, H., Jahnke, G., and Ben-Zion, Y. (2002). Numerical simulation of fault zone guided waves: Accuracy and 3-D effects. *Pure appl. geophys.*, 159(9):2067–2083.

Karrenbach, M. (1995). *Elastic tensor wave fields*. PhD thesis, Stanford University.

Kebeasy, T. R. M. and Husebye, E. S. (2003). A finite-difference approach for simulating ground responses in sedimentary basins: quantitative modelling of the Nile Valley, Egypt. *Geophys. J. Int.*, 154(3):913–924.

Kravtsov, Y. A. and Orlov, V. I. (1990). *Geometrical optics of inhomogeneous media*. Springer Verlag, Berlin.

Lecomte, I., Gjøystdal, H., Drottning, Å., Maaø, F. A., Johansen, T. A., and Bakke, R. (2004). Efficient and flexible seismic modeling of reservoirs: A hybrid approach. *The Leading Edge*, 23(5):432–437.

Martin, M., Ritter, J. R. R., and the CALIXTO working group (2005). High-resolution teleseismic body-wave tomography beneath se romania - I. Implications for three-dimensional versus one-dimensional crustal correction strategies with a new crustal velocity model. *Geophys. J. Int.*, 162(2):448–460.

Martin, M., Ritter, J. R. R., and the CALIXTO working group (2006). High-resolution teleseismic body wave tomography beneath SE-Romania - II. Imaging of a slab detachment scenario. *Geophys. J. Int.*, 164(3):579–595.

Miksat, J. (2006). *Earthquake Ground Motion Modelling from Crustal and Intermediate Depth Sources*. PhD thesis, Karlsruhe University.

Miksat, J., Wenzel, F., and Sokolov, V. (2005). Low free-field accelerations of the 1999 Kocaeli earthquake? *Pure appl. geophys.*, 162(5):857–874, doi:10.1007/s00024–004–2645–8.

Olsen, K. B. (1994). *Simulation of three-dimensional wave propagation in the Salt Lake Basin*. PhD thesis, University of Utah, Salt Lake City.

Olsen, K. B. (2000). Site amplification in the Los Angeles basin from three-dimensional modeling of ground motion. *Bull. Seism. Soc. Am.*, 90(6B):S77–S94.

Olsen, K. B., Pechmann, J. C., and Schuster, G. T. (1996). An analysis of simulated and observed blast records in the Salt Lake Basin. *Bull. Seism. Soc. Am.*, 86(3):1061–1076.

Oth, A., Wenzel, F., and Radulian, M. (2007). Source parameters of intermediate-depth Vrancea (Romania) earthquakes from Empirical Green's Functions modeling. *Tectonophysics*, 438(1-4):33–56, doi:10.1016/j.tecto.2007.02.016.

Vidale, J. and Helmberger, D. V. (1987). *Seismic Strong Motion Synthetics*, chapter Path effects in strong motion seismology, pages 267–319. Computational Techniques. Academic Press Inc, London.

Vidale, J., Helmberger, D. V., and Clayton, R. W. (1985). Finite-difference seismograms for SH waves. *Bull. Seism. Soc. Am.*, 75(6):1765–1782.